IEEE Access
Multidisciplinary | Rapid Review | Open Access Journal

Received June 24, 2020, accepted July 3, 2020, date of publication July 7, 2020, date of current version July 17, 2020.

Digital Object Identifier 10.1109/ACCESS.2020.3007718

Design, Prototyping and Testing of a Rotating Electrical Machine With Linear Geometry for Shipboard Applications

MARIO MEZZAROBBA[1], ALBERTO TESSAROLO[1], (Senior Member, IEEE), NICOLA BARBINI[1], SIMONE CASTELLAN [1], BARBARA CODAN[2], MARTINA TERCONI[3], CLAUDIO BRUZZESE[4], (Senior Member, IEEE), AND AUGUSTO FUSARI[5]

[1]Department of Engineering and Architecture, University of Trieste, 34127 Trieste, Italy
[2]Lampas System, 34015 Muggia, Italy
[3]Area Science Park, 34149 Trieste, Italy
[4]Department of Astronautic, Electrical, and Energy Engineering, Sapienza University of Rome, 00185 Rome, Italy
[5]ABB, 20099 Sesto San Giovanni, Italy

Corresponding author: Alberto Tessarolo (atessarolo@units.it)

This work was supported by the Friuli Venezia Giulia Regional Authority through Programma Operativo Regionale – Fondo Europeo di Sviluppo Regionale (POR-FESR), European Regional Development Fund (ERDF) Funding, under Activity 1.3.b, 2014–2020 Program.

ABSTRACT Conventional rotating electrical machines are characterized by stator and rotor structures featuring a cylindrical geometry around the shaft rotational axis. Although advantageous for mechanical reasons, the cylindrical geometry results in overall machine shapes and dimensions that may be unsuitable for installation. This particularly occurs in shipboard applications, where electric motors and generators are subject to stringent room constraints and need to be fit in unusually shaped compartments. This paper presents the development and test of a dual-shaft rotating permanent-magnet electric machine prototype having a linear structure that facilitates its onboard use for such applications as electric propulsion and rudder actuation. In fact, the proposed machine topology has overall dimensions which can be adjusted to fit the space available for installation. The operating concept and the detailed electromechanical design of the machine are first described. Then the manufacturing and factory test of the prototype under inverter supply are illustrated. Finally, the validation of the prototype as a boat propulsion variable-speed inverter-fed motor is presented. It is proved that, despite of its highly non-conventional electromechanical design, the machine can be effectively fed from a general-purpose inverter for permanent magnet motors.

INDEX TERMS Direct-drive actuators, electromagnetic design, finite element analysis, linear electric machines, permanent-magnet machines, ship propulsion, shipboard applications, variable-speed drives.

I. INTRODUCTION

The characteristic dimensions D and L of the outer cylindrical envelop that encloses a conventional rotating electric machines, depicted in Figure 1-a, strongly depend on the machine ratings and number of poles. In general, the overall volume of permanent magnet machines, hence the D^2L product, increases with the rated torque [1], while the D/L ratio tends to grow with number of poles [2]. As a consequence, high-torque low-speed motors and generators may have a large diameter D which makes their installation prohibitive in presence of room restrictions. On the order side, we can notice that in some cases, such as in shipboard applications, electric motors and generators need to be fit into small and unusually shaped vanes leading to very strict constraints on the electric machine height, width and length.

Possible ways to cope with space constraints is to use high-speed machines with gear-boxes [3], which are, however, know to suffer from reliability, and maintenance issues [3], [4]. Another solution is represented by hydraulic actuators which, however, may suffer from heavy maintenance, working-fluid leakages [5] and cumbersome equipment for pressurized oil supply. [6], [7].

The associate editor coordinating the review of this manuscript and approving it for publication was Shihong Ding.

The adoption of a full-electric direct-drive solution – with all the efficiency, maintenance and reliability benefits described in [7] – would be highly facilitated in presence of strict space restrictions if the electric machine geometry could be changed and adjusted to the dimensions available for installation. This paper investigates the possibility to effectively achieve such purpose by means of a new kind of permanent-magnet electric machine design, characterized by the linear configuration schematically depicted in Figure 1-b., where the three dimensions H, L and W can be changed, to a certain extent, to fit the application and dimensional constraints. The basic idea and working principle of the new rotary machine with linear structure was first presented in [8], along with its implementation into an initial rudimentary prototype. The prototype in [8], however, could be tested only as a driven generator with very light loads because of large vibrations and very noisy operation. Unacceptable mechanical wear of rotating parts was also observed. After the experience reported in [8], in fact, serious doubts remained about the possibility to use the new design for practical applications.

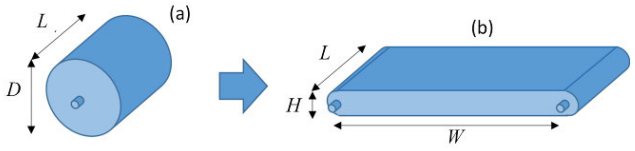

FIGURE 1. (a) Conventional rotating machine geometry. (b) New rotating machine with linear configuration.

As a follow-up and substantial advancement of the work presented in [8], this paper illustrates, for the first time in the literature, a detailed method and technology to successfully design a rotating electric machine with linear geometry and its implementation into a full-scale technology demonstrator tested in its final destination operating environment. The substantial advances with respect to [8] are listed next.

Firstly, the initial design of the machine is radically reviewed to achieve a smooth and quiet mechanical operation. For this purpose, the outer rotor structure is completely changed introducing a new method for mechanically connecting its elements by means of chains and rolling bearings. Calculations are reported to support the reasons for the design change and the criteria followed, as well as to quantify the expected improvements.

Secondly, the implementation of the reviewed design into a full-scale prototype, conceived for boat propulsion purposes, is described.

Thirdly, the manufacturing and successful factory and field test of the prototype as a boat propulsion inverter-fed motor are reported to prove the feasibility of the new design solutions proposed and their effectiveness in terms of satisfactory machine performance.

The paper is organized as follows. In Section II the basic structure and operating principle of the rotating linear machine is described, along with possible shipboard application scenarios. In Section III the design of the machine prototype is addressed, in regards to both electromagnetic and mechanical aspects. Section IV reports on the prototype construction and the issues found in its fabrication. Section V describes the testing activity conducted on the prototype both in a factory and laboratory environment and during its operation as boat propulsion variable-speed inverter-fed motor.

II. BASIC IDEA AND POSSIBLE APPLICATIONS

A. MACHINE STRUCTURE AND OPERATING PRINCIPLE

The basic structure of the machine is illustrated in Figure 2.

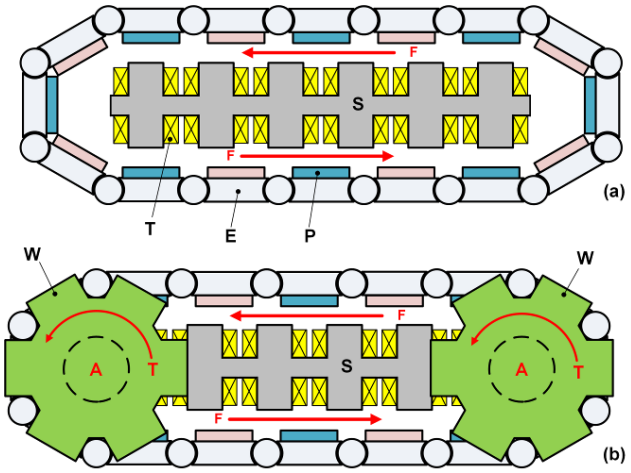

FIGURE 2. Basic structure of the rotating electric machines with linear topology: (a) wound stator and track-like rotor; (b) force to torque conversion through tooth-wheels.

It consists of an outer permanent-magnet rotor designed in the form of a continuous track. The continuous track is composed of a band of connected ferromagnetic elements (E), each carrying a permanent magnet (P) in its inner side. Adjacent elements bear permanent magnets with opposite magnetization direction. The stator part is basically the same as in a double-sided permanent-magnet linear synchronous motor equipped with a fractional-slot concentrated winding [9]. It consists of a ferromagnetic laminated core (S) wound with tooth coils (T). When energized with a three-phase current system, the stator produces a travelling magnetic field (F) which drags permanent magnets causing the continuous track motion. By mechanically connecting the continuous track to a tooth wheel (W), the developed linear force is converted into torque applied to rotary shafts (A). The machine is obviously reversible and can operate as a generator if the electrical and mechanical power flows are reversed. Furthermore, the machine is naturally suitable for being coupled to two parallel shafts rotating at the same speed and in the same direction. Depending on the application, either one or both of the two shafts can be used to connect the machine to the coupled rotating equipment.

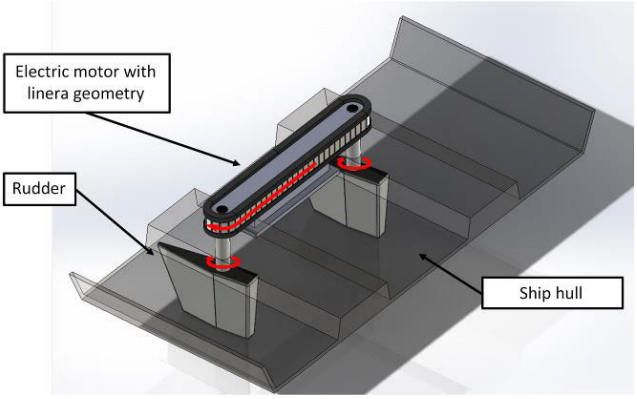

FIGURE 3. Application of the rotating motor with linear geometry as a ship rudder electric actuator.

B. POSSIBLE APPLICATIONS IN THE SHIPBOARD ENVIRONMENT

A possible application in the shipboard environment is rudder actuation as illustrated in Figure 3, where the dual-shaft rotating motor is used to synchronously steer the two parallel-axis rudders. This would be a fully-electric alternative to the presently-used hydraulic technology shown in Figure 4, where hydraulic vane motors (V) or hydraulic cylinders (H) are employed to apply the needed torque to rudder shafts (R), while synchronism between the two rudders is guaranteed by a synchronizing bar (S). While vane motors and hydraulic cylinders are very compact, their operation needs cumbersome equipment for the storage, processing and adduction of pressurized oil (Figure 5). Such equipment is also subject to frequent leakages from pipes [5] and requires considerable maintenance. Furthermore, the need to keep the oil in pressure even when actuators are at no load implies the use of continuously-running motor-driven pumps which cause large electric energy consumption [10].

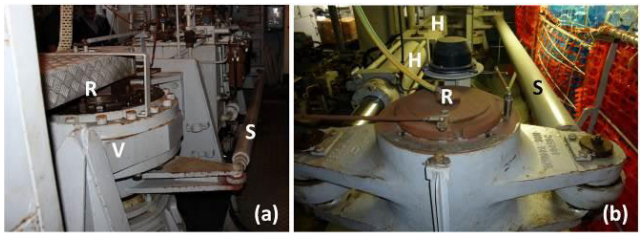

FIGURE 4. Presently used hydraulic technologies for rudder actuation: (a) with rotary vane motors; (b) with hydraulic cylinders.

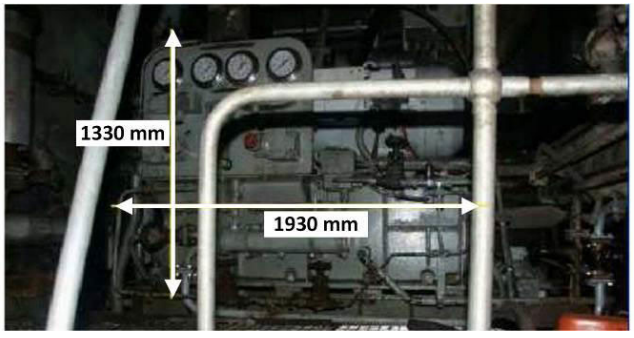

FIGURE 5. Example of shipboard equipment for pressurized oil storage and processing.

All these disadvantages could be overcome using a full-electric direct-drive solution as explained in [7]. Various technologies can be potentially adopted for rudder steering system electrification (Figure 6). The most traditional solution consists of using a conventional rotary torque motor directly coupled to each rudder shaft (M). However, due to the large torques needed [11], the size and weight of the conventional rotary motor would be prohibitive for mounting on shaft rudder axes. The use of a permanent-magnet synchronous linear motor (L) with the stator fixed to the ship hull and the mover coupled to rudder shafts through tillers (T), in lieu of the synchronizing bar (Figure 4), is proposed in [7]–[11]. Although promising, the solution may be critical in some applications as it requires long tillers to convert the thrust developed by the linear motor (L) into the the required steering torque [11].

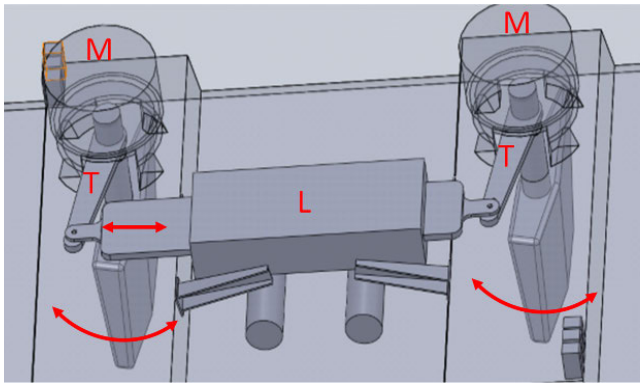

FIGURE 6. Full-electric solutions for direct-drive rudder actuation based on conventional rotating motors (M) or linear motors (L).

The adoption of the rotating motor with linear topology addressed in this paper (Figure 3) retains the advantage of fully exploiting the space between rudder shafts as allowed by the conventional linear motor but removes the need for long tillers. The motor can be, in fact, installed along the line connecting rudder axes, thus filling a space which is usually unexploited. On the other hand, unlike conventional rotary motors, the rotating machine with linear topology leads to easier installation as it can be fixed to the ship hull structure between the two rudders so that its weight is borne by a relatively large bearing surface.

Another possible shipboard application is the full-electric direct-drive steering of stabilizing fins which are mounted on the side of the hull (Figure 7) and used for continuous adjustment of ship attitude.

Stabilizing fins are usually driven by hydraulic actuators. In order to overcome the mentioned issues relating to the use

FIGURE 7. (a) Stabilizing fins for a naval vessel and (b) detail of the skull-mounted hydraulic steering system.

of pressurized oil on board, full-electric direct-drive solutions based on linear electric motors have been proposed [12], as conceptually illustrated in Figure 8. The need for a tiller to transform the linear thrust into rotary torque (Figure 8) can be removed if the rotating electric motor with linear topology is used as an alternative, as shown in Figure 9, leading to a flexible solution also thanks to the possibility to choose among different possible mounting arrangements based on the space available for installation.

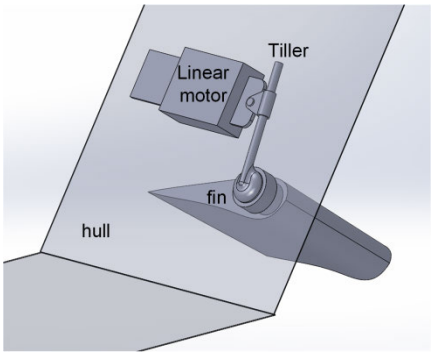

FIGURE 8. Possible full-electric direct-drive solution for stabilizing fin steering by means of a linear motor.

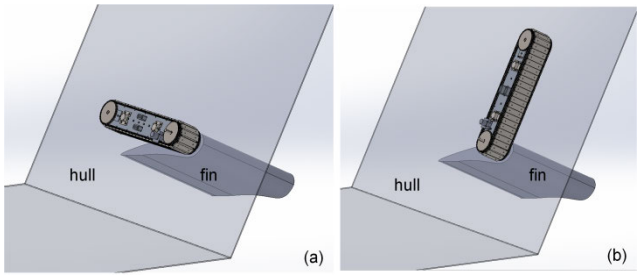

FIGURE 9. Possible full-electric direct-drive solution for stabilizing fin steering by means of a rotary motor with linear topology with different mounting arrangement: (a) horizontal; (b) vertical.

Further applications of the proposed motor topology to shipboard drives, including propulsion, are possible, as it will be illustrated by the testing activity of the machine prototype described next.

III. PROTOTYPE DESIGN

In this Section, the design of a prototype for the proposed rotating electric motor with linear topology is illustrated, addressing both electromagnetic and mechanical aspects.

A. MECHANICAL DESIGN

The mechanical design is based on the lessons learnt from the construction and testing on the initial proof-of-concept rudimentary prototype described in [8] and briefly recalled next.

1) ISSUES OBSERVED IN THE ORIGINAL PROOF-OF-CONCEPT PROTOTYPE

The original machine built and tested for proof-of-concept purposes [8] implemented the basic operating principle described in II.A in the simplest possible manner as shown in Figure 10: the outer permanent-magnet rotor was composed of a sequence of ferromagnetic elements (E) bearing permanent magnets (M) and connected through hinge joints. All hinge joints had pins (P) that, in addition to connecting trach elements, hanged out on the two sides and interlocked with the toothed wheels thus transferring the linear force developed on the track into torque applied to the revolving shafts. While travelling between the two wheels, the pins were expected to slide and roll along linear guides (G), formed by the edges of the machine side shields, so as to guarantee a uniform air gap between the permanent magnets and the inner stator core (S).

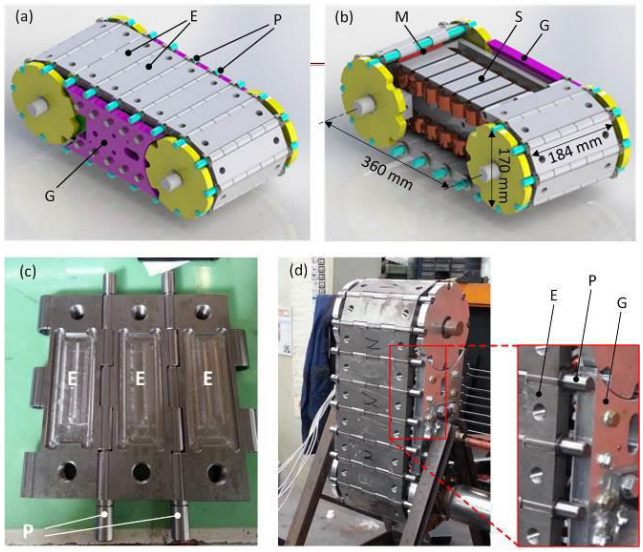

FIGURE 10. Mechanical design of the original prototype: (a)-(b) 3D renderings; (c) track elements and hinges before magnet assembly; (c) machine under testing.

During testing, significant vibrations and noise occurred and a mechanical wear of rotating parts was observed even after a short time of operation as a driven generator at no load. This prevented the machine from being tested at full load and in motoring mode. A subsequent root-cause-analysis revealed that the malfunctioning originated from two main problems.

The first problem is illustrated in Figure 11: due to the air-gap magnetic field, permanent magnets are attracted by the ferromagnetic stator with a force F_m, which necessarily results in forces F_p applied, inside hinge joints, to each pin.

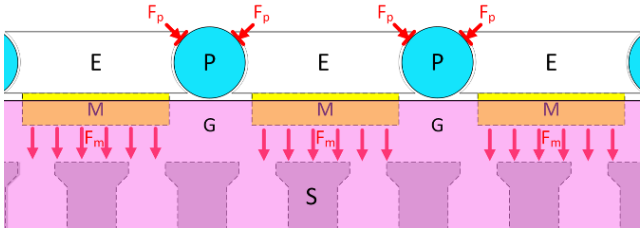

FIGURE 11. The attraction force (F) between the permanent magnets (M) and the stator core (S) causes a pressure (P) between the hinges (H) and the sliding guides (G).

The forces F_p determine a significant friction that prevents pins from freely rolling inside hinges and from smoothly sliding along linear guides.

The second problem relates to the kinematics of the outer rotor motion. To describe it, let us consider the example geometric model shown in Figure 12, where each wheel has $Z = 6$ teeth. The portion of the machine comprised between the two wheel axes a_1 and a_2 can be defined as the "active region" because it is the part where the force develops on the outer rotor due to the interaction between the permanent magnets and the stator magnetic field. In the active region, in fact, the stator core with its electric windings is placed (Figure 10b). While travelling through the active region, the rotor pins are forced to slide on linear guides (Figure 10), thus moving along two straight lines ℓ_{top} and ℓ_{bottom}. This makes it possible to have a uniform distance g (air gap) between the permanent magnets and the stator core. Conversely, when the pins engage with the toothed wheels, they are forced to move along circumferential arcs Γ_1 and Γ_2.

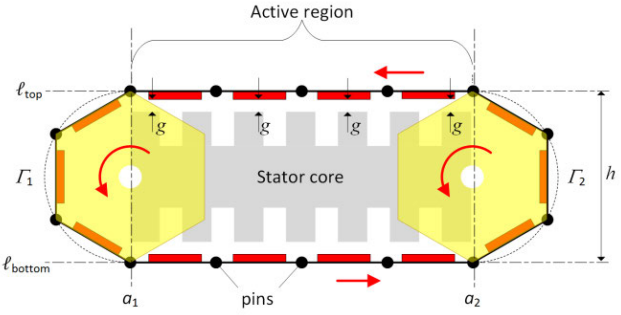

FIGURE 12. While traveling through the active region, pins are forced by linear guides to move along straight lines ℓ_{top} and ℓ_{bottom} so that a uniform air gap g between the magnets and the stator core is maintained. After engaging with the toothed wheels, instead, pins are forced to move along circumferences Γ_1 and Γ_2.

If linear guides were not used, the outer rotor would revolve as a normal continuous track as illustrated in Figure 13a. Under this hypothesis, the length of the track would naturally be the same for all wheel positions, but the air gap would change. For example, when passing from one wheel position to another, the pins at points P_{1a}, P_{1b}, P_{2a}, P_{2b} would respectively move to points P'_{1a}, P'_{1b}, P'_{2a}, P'_{2b}leading the air gap to reduce by Δg. On the other hand, if linear guides are used (Figure 13b), pins are always forced to slide along the same straight lines ℓ_{top} and ℓ_{bottom} while traveling in the active region of the machine.

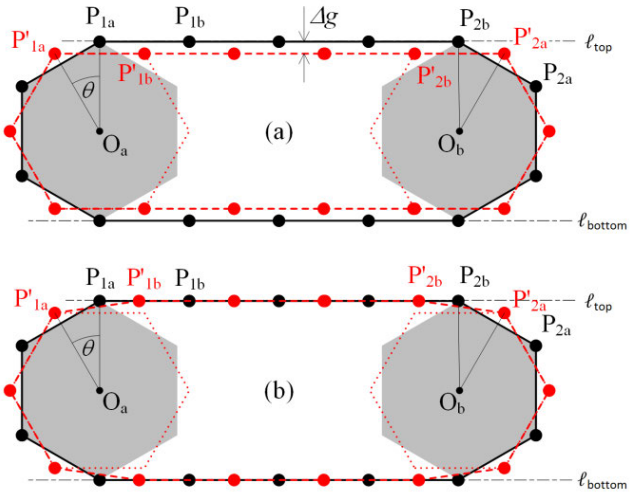

FIGURE 13. Positions of outer rotor elements at a given instant (continuous black line) and after the wheels have rotated by an angle θ (dashed red line). (a) Case where no linear guide is used; (b) case where linear guides force pins to move along lines ℓ_{top} and ℓ_{bottom}.

This guarantees a uniform air gap, but implies the length of the track to vary from one instant to the other. As a consequence, the track is stretched and forced to slightly increase its length. Of course, the two situations illustrated in Figure 13b repeat alternately each time the wheels rotate by half a tooth pitch, causing a pulsating tensile stress that inevitably results in noise and vibration effects, as well as rotating track mechanical wear.

It is evident from Figure 13 that, for a generic design of the machine, the higher the number of teeth Z in the toothed wheels the lower the periodic elongation Δ imposed on rotor track elements will be.

In order to quantify the elongation Δ, we can refer to Figure 13b. For example, let us consider the four pins moving from positions P_{1a}, P_{1b}, P_{2a}, P_{2b} into positions P'_{1a}, P'_{1b}, P'_{2a}, P'_{2b}, when the wheels rotate by an angle θ in counterclockwise direction. In the ideal case with no linear guides (Figure 13a), the distances $P_{1a}-P_{1b}$, $P_{2a}-P_{2b}$, $P'_{1a}-P'_{1b}$, $P'_{2a}-P'_{2b}$ remain equal to the tooth pitch, i.e.:

$$\overline{P_{1a}P_{1b}} = \overline{P_{2a}P_{2b}} = \overline{P'_{1a}P'_{1b}} = \overline{P'_{2a}P'_{2b}} = h \sin\frac{\pi}{Z} \quad (1)$$

where h is the diameter of the wheels (Figure 12) and π/Z is half the wheel tooth pitch angle. Conversely, from simple geometric considerations applied to Figure 13-b (where linear guide effects are considered), we can write the identities (2) and (3) for the pins on the left-hand and right-hand side, respectively:

$$\overline{P'_{1a}P'_{1b}}^2 = \left(\frac{h}{2}\sin\theta + \overline{P_{1a}P_{1b}} - \overline{P'_{1b}P_{1b}}\right)^2 + \left(\frac{h}{2} - \frac{h}{2}\cos\theta\right)^2 \quad (2)$$

$$\overline{P'_{2b}P'_{2a}}^2 = \left[\overline{P'_{2b}P_{2b}} + \frac{h}{2}\sin\left(\frac{2\pi}{Z} - \theta\right)\right]^2 + \left[\frac{h}{2} - \frac{h}{2}\cos\left(\frac{2\pi}{Z} - \theta\right)\right]^2 \quad (3)$$

For a conservative estimation, let us suppose that only one track elements bears all the elongation impressed on the whole track. Under this assumption, the elements corresponding to segments $\overline{P'_{1a}P'_{1b}}$, $\overline{P'_{2b}P'_{2a}}$ and $\overline{P_{1a}P_{1b}}$ retain their length given by (1). We can then substitute (1) into (2) and (3), finding

$$\overline{P'_{1a}P_{1b}} = h\left[\frac{1}{2}\sin\theta + \sin\frac{\pi}{Z} - \sqrt{\sin^2\frac{\pi}{Z} - \frac{(1-\cos\theta)^2}{4}}\right] \quad (4)$$

$$\overline{P'_{2b}P_{2b}} = h\left[\sqrt{\sin^2\frac{\pi}{Z} - \frac{\left(1-\cos\left(\frac{2\pi}{Z}-\theta\right)\right)^2}{4}} - \frac{1}{2}\sin\left(\frac{2\pi}{Z}-\theta\right)\right] \quad (5)$$

If no elongation occurred, $\overline{P'_{1a}P_{1b}}$ and $\overline{P'_{2b}P_{2b}}$ given by (4) and (5) would be equal. Instead, the maximum elongation Δ_{max} to which a single track element can be subject is given by their difference, i.e.:

$$\Delta_{max} = \left|\overline{P'_{2b}P_{2b}} - \overline{P'_{1a}P_{1b}}\right| = h\left[\begin{array}{l}\frac{1}{2}\sin\left(\frac{2\pi}{Z}-\theta\right) - \sqrt{\sin^2\frac{\pi}{Z} - \frac{1}{4}\left[1-\cos\left(\frac{2\pi}{Z}-\theta\right)\right]^2} \\ +\frac{1}{2}\sin\theta + \sin\frac{\pi}{Z} - \sqrt{\sin^2\frac{\pi}{Z} - \frac{1}{4}\left[1-\cos(\theta)\right]^2}\end{array}\right] \quad (6)$$

For the original prototype design (Figure 10b, $Z = 8$), the diagram of $\Delta_{\max}$ as a function of θ according to (6) is plotted in Figure 14.

We can observe that each element of the outer rotor track, while moving through the active region, is subjected to a pulsating traction force that tends to change its length by a quantity which can reach 0.65 mm each time the wheels rotate by a tooth pitch angle. This fully explains the unsatisfactory mechanical behavior of the original prototype described in [8].

2) PROTOTYPE RE-DESIGN

The new proposed design of the machine, intended to overcome or reduce the mechanical issues highlighted in the previous subsection, is illustrated in Figure 15, with relevant dimensions given in Table 1.

The basic structure of the machine is still equipped with an outer track-like rotor consisting of several ferromagnetic

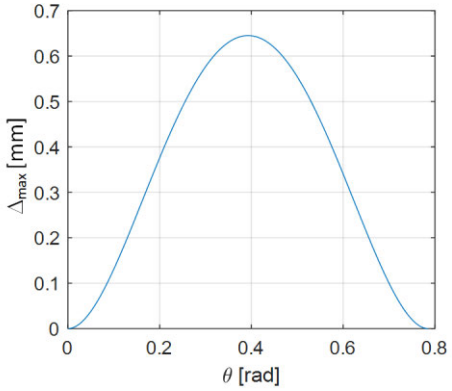

FIGURE 14. Elongation Δ_{max} as a function of the wheel rotation angle θ ($0 \le \theta \le 2\,\pi/Z$) for $Z = 8$.

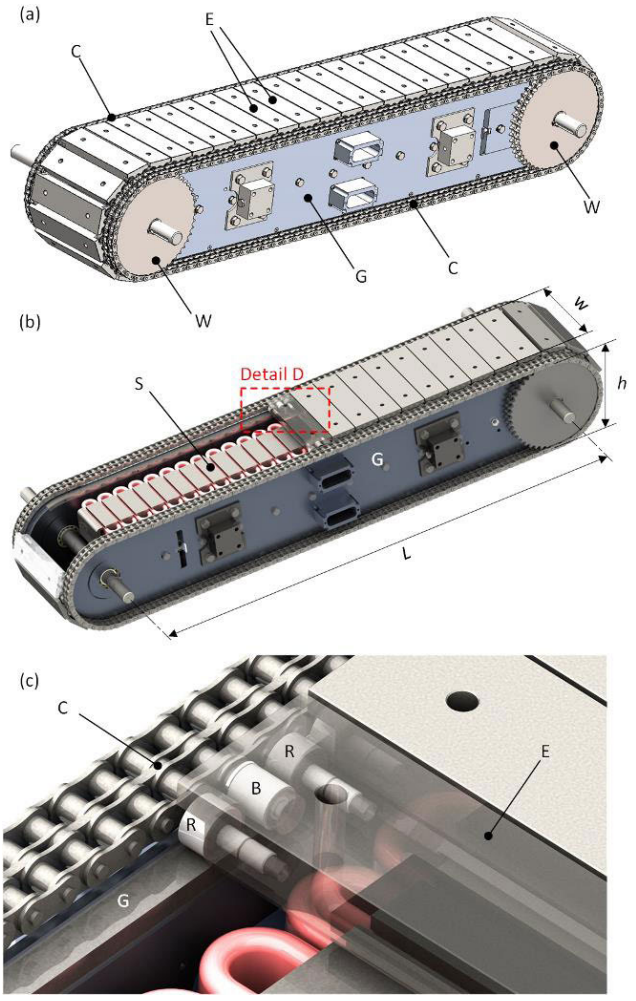

FIGURE 15. 3D rendering of the new prototype design. (a) Complete machine view; (b) view after removal of some outer rotor element; (c) detail D of the previous sub-figure.

elements (E), each carrying a permanent magnet, and with an inner stator (S) with concentrated-coil tooth windings. The basic difference is that, in the new proposed design, the rotor elements are not connected through hinge joints, but through

TABLE 1. Machine characteristic dimensions [1].

L	1200 mm	h_m	8 mm
w	218 mm	h_y	27 mm
h	283 mm	h_t	40 mm
w_m	100 mm	h_{tt}	6 mm
g_y	2 mm	g	5 mm
L_e	61.5 mm	τ_s	42.33 mm
L_m	40 mm	s_o	2 mm

[1] Some of dimensions refer to design details which will be illustrated later on (Figure 17)

chains (C). The same chains which connect the rotor elements are designed to engage with the toothed wheels (W) to convert the linear thrust into torque. As it happened in the original prototype, when moving in the active region of the machine the ferromagnetic elements slide on linear guides (G), which guarantees a uniform air gap. Linear guides are still constituted by the edges of the side shields that enclose and support the inner stator core, as explained further on in more detail.

An insight into the design of a single rotor element and its interface with the rest of the machine is provided in Figure 15c and Figure 16.

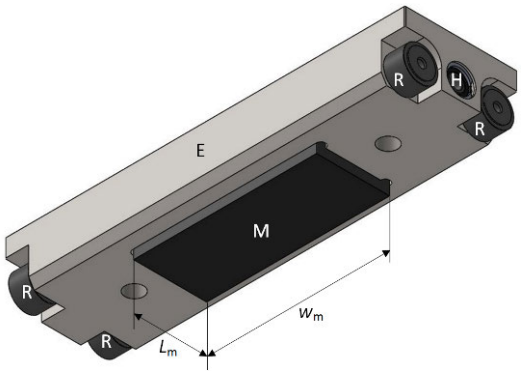

FIGURE 16. 3D rendering of a single ferromagnetic element of the outer rotor track for the new prototype.

The track element is equipped with four rollers (R) which enable it to slide along linear guides (G). Between the rollers, a threaded hole (H) is machined for insertion of roller bearings (B) which connect the element to the chains as illustrated in Figure 15c. It is worth noticing that there is no direct mechanical connection between elements, which are all individually and independently connected to the chains. This enables them to freely rotate by different angles (within proper ranges) around the axes of their respective roller bearings (B).

The new design is suitable for solving the mechanical issues identified in the original prototype implementation (III.*A*.1). In fact, rollers (R) are selected as off-the-shelf industrial components proven and guaranteed to withstand the attraction force F_m (Figure 11) between each element and the stator core with a significant safety margin (larger than 300%). Furthermore, the use of chains as mechanical interfaces to interlock the outer rotor track with toothed wheels makes it possible to select a very large number of teeth Z per wheel.

With the original prototype design (Figure 10) adapted to the larger dimensions given in Figure 15b, we would have $Z = 12$ teeth on each wheel and, according to (6), the maximum elongation, Δ_{max} for each track element would be 0.32 mm, which is still very high. Conversely, with the new proposed prototype design it is possible to raise the number of teeth per wheel to $Z = 48$ and, in such case, (6) yields a maximum length variation around 5μm for all the revolving components of the rotor. Such elongation can be borne by all elements with almost negligible mechanical stress thanks to the intrinsic elasticity of the employed ferromagnetic material (ISO 10 B-2 steel).

For the sake of clarity and completeness, Figure 17 shows a partial cross-sectional view of the machine, including both stator and rotor active parts, with relevant dimensions provided in Table 1. Regarding the stator part, its overall implementation is shown in Figure 18. The stator consists of two laminated cores (one on the upper and the other on the lower side), each wound with concentrated tooth coils.

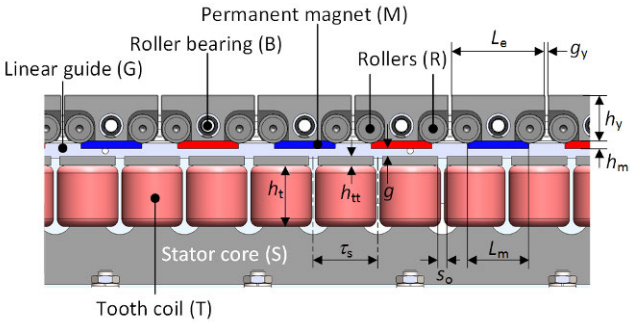

FIGURE 17. Cross-sectional view of stator and rotor active parts showing the mechanical air gap g, the magnetic air gap g_m and the yoke air-gap g_y.

As better specified in the next Section, the windings are designed so that, when fed with a symmetrical three-phase current system, they produce travelling fields that move in opposite directions on the upper and lower active regions of the machine, as required to maximize the net magnetic force acting on the track and transformed into torque (Figure 2b). The use of a fractional-slot concentrated winding (FSCW) [13] instead of a conventional distributed topology [14] is particularly beneficial thanks to its very short winding overhangs to limit the machine dimension called W in Figure 15-b. The two stator laminated cores are fixed on a non-magnetic stainless-steel support (Figure 18) which has a basically structural function as it serves to firmly connect the stator to the side shields (G in Figure 15) on whose edges the outer rotor elements slide. The use of a non-magnetic material helps to have the two (upper and lower) sides of the machine work independently, preventing the magnetic flux from flowing between the two cores; furthermore, it limits the occurrence of additional losses due to eddy currents produced by leakage fluxes [15].

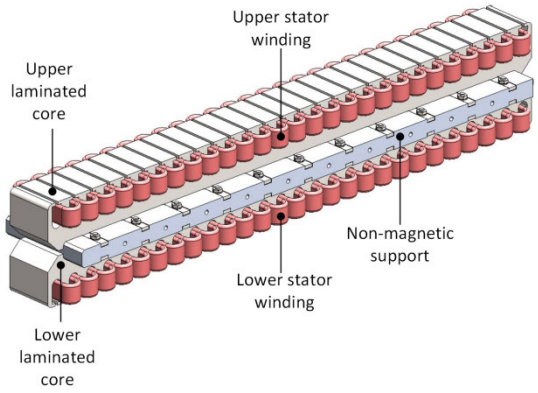

FIGURE 18. 3D rendering of the machine stator core and winding.

B. ELECTROMAGNETIC DESIGN

Although it is herein treated separately for the sake of clarity, the electromagnetic design of the prototype is tightly connected with its mechanical design. In fact, throughout the machine development process, it has been necessary to continuously adjust electromagnetic details for structural reasons and, on the other hand, to select the mechanical arrangement to improve the electromagnetic performance.

The optimal electromagnetic solution finally chosen to fit the mechanical stator and rotor structure illustrated in the previous Section is that of a surface-mounted permanent-magnet (SPM) fractional-slot concentrated winding (FSCW) machine according to the scheme shown in Figure 19.

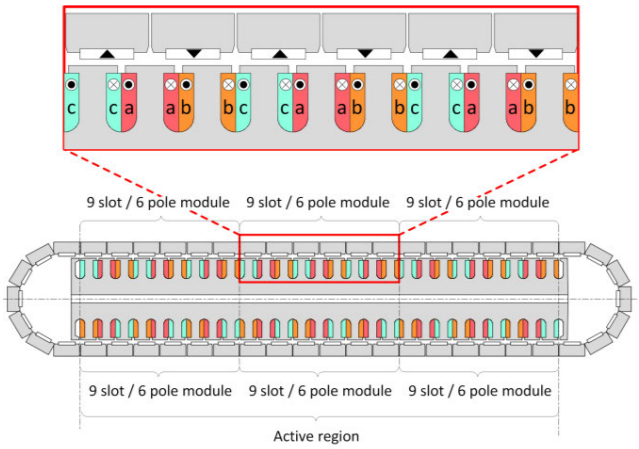

FIGURE 19. Cross-sectional view of stator and rotor active parts where different colors are used for the three stator phases and symbols ⊗ and ⊙ are used to denote different phase current conventional directions.

The revolving track corresponds to the SPM rotor where permanent magnets are mounted with alternating magnetization directions in successive track elements such that each element constitutes one rotor pole. Therefore, the machine has an overall number of poles equal to 50. However, the active region of the machine, where the electromechanical energy conversion takes place, comprises 36 poles, of which 18 are on the upper and 18 on the lower side.

The active region has a modular structure in the sense that it consists of six dual-layer FSCW modules, each composed of 9 teeth and 6 poles [15]. Figure 19 illustrate the subdivision of the machine electromagnetic structure into modules and shows the detailed arrangement of the phases across the single module. As in all FSCW machines, the modularity could be exploited to improve fault tolerance: this would be possible by independently supplying the six modules with separate in-phase electrical sources so that, in case of a fault in either a module or supply source connected to it, the faulty module can be disconnected while the machine can remain in service with the healthy modules supplied [16]. For the design of the specific prototype under investigation, all the phases of the stator winding module are series-connected so that the machine can be supplied using only one Voltage Source Converter (VSC).

The number of turns per tooth coil is chosen equal to 17 so as to have a rated line-to-line rms voltage of 380 V.

Example of design choices which had to be made from the electromagnetic standpoint are the selection of the slot opening width s_o (Figure 17) and the stator core end shaping. By FEA simulations, these two factors have been, in fact, found to significantly affect the cogging torque, as illustrated in Figure 20.

Figure 20-a shows how the cogging torque amplitude varies for different shapes of the stator core end. The variation can be explained considering that a part of the cogging torque results from the interaction between the core end and the magnets which are travelling outside the active region of the machine (Figure 21-a). The analysis illustrated in Figure 20-a shows that a rectangular configuration of the stator core (i.e. with no rounding of end parts) is the most favorable in terms of cogging torque minimization and, for this reason, it has been assumed in the final prototype design.

Figure 20-b shows that the smaller the slot opening the lower the cogging torque will be. This has led to select a slot opening width of 5 mm which is the smallest value compatible with manufacturing constraints.

The analyses shown in Figure 20 refer to no-load operation. The electromagnetic performance of the machine in different operating conditions can be investigated by FEA simulations as well. The main challenge in this task is modeling the outer rotor motion, which is partly linear and partly circular, while most of commercial FEA software packages are capable of accounting for either circular or linear motion, but not for both at the same time. Representing the kinematics of the outer rotor therefore implied the use of dedicated scripts to locate all the single track elements in the right place and with the right orientation for any given position of the toothed wheels.

Examples of solved electromagnetic FEA models are shown in Figure 21, for both no-load and loaded operation.

It can be clearly observed from Figure 21 how the magnetic flux produced by permanent magnets, stator current

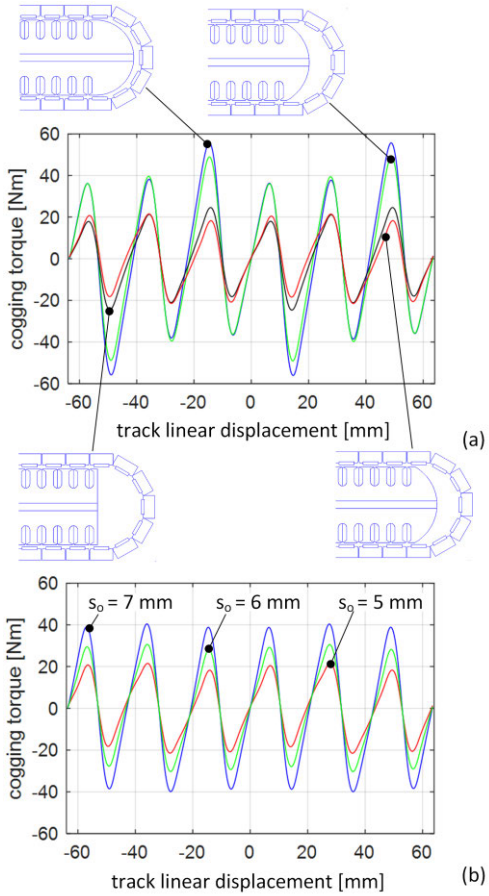

FIGURE 20. Cogging torque as a function of the rotor linear displacement: (a) for a slot opening $s_o = 5$ mm and different stator core end shaping; (b) for rectangular stator core shape and different values of the slot opening s_o.

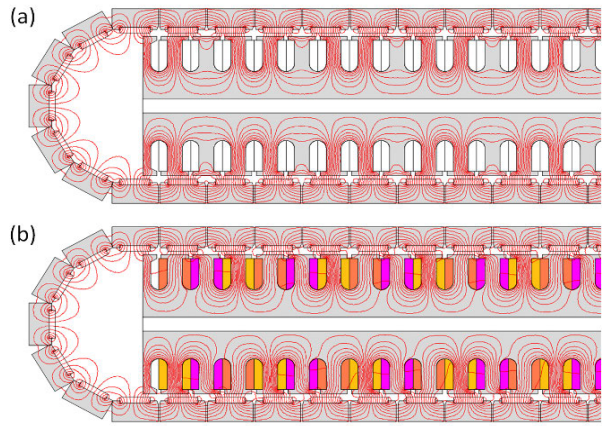

FIGURE 21. Examples of electromagnetic FEA simulations of the prototype: (a) at no load; (b) in loaded conditions.

or both flows through the air gap, the permanent magnets, the stator teeth, the stator yokes and the ferromagnetic portion of the track elements, which therefore act as rotor yokes or back iron. In conventional machines (whether rotating or linear) both stator and rotor yokes are continuous. For the prototype under study, instead, the rotor back iron is necessarily segmented because a certain air gap needs to exist between adjacent track elements (Figure 17) to avoid contact and friction in case of small track deformations. Of course, the small air gap between adjacent elements increases the reluctance of the magnetic flux paths, thus reducing the flux density with respect to a conventional machine with continuous back iron. However, this reduction effect is practically negligible because, as it can be seen from Figure 21, each flux line crosses the main air gap twice and the air gap between adjacent elements only once. Therefore, considering that the relative magnetic permeability of permanent magnets is very close to that of the air [15], the relative increase in the reluctance due to the discontinuous rotor structure with respect to a continuous back iron is

$$\left[g_y + 2\left(h_m + g\right)\right] / \left[2\left(h_m + g\right)\right], \tag{7}$$

which is equal to 108% with symbols and dimensions showed in Figure 15 and 17 and Table 1. Of course, the possibility to accept a magnetically discontinuous rotor back iron without significant derating effects is a direct consequence of choosing a FSCW. In fact, if a distributed winding were used the flux lines would be force to flow through the rotor back iron along much longer paths passing from one element to the adjacent one several times and this would lead to higher magnetic voltage drops due to the gaps between rotor elements.

C. THERMAL DESIGN AND MACHINE RATINGS

In the development of a prototype with a higher technology readiness level, thermal and heat transfer aspects should be considered along with mechanical and electromagnetic issues. Due to time and budget constraints, however, the design of a suitable cooling system could not be addressed for the prototype machine under study, the main target of the project being the mechanical design improvement of the initial proof-of-concept prototype in view of shipboard applications.

It can be envisioned, though, that the particular structure of the machine makes it suitable for being equipped with an effective cooling system, for example using the non-magnetic support between the two stator cores (Figure 19) as a heat sink to be cooled through an integrated water heat exchanger. Also, the side shields (G) can be easily equipped with inlet and outlet ducts for cooling air forced circulation.

Of course, the electrical loading of the machine and hence the torque it can produce strongly depends on the cooling system effectiveness. Therefore, in absence of a detailed cooling system design it does not make sense to specify machine nameplate data in terms of torque and power capability at a given speed.

For the purpose of the factory, laboratory and shipboard testing activities, the working point has been thus determined so as to avoid overheating in presence of a cooling system based on natural convection only. Regarding the rotational

speed, the application of the machine as a boat propulsion motor required a variable speed changing from zero to around 1000 r/min. Under such constraints, the machine has been operated assuming the reference performance data listed in Table 2.

TABLE 2. Reference performance data assumed for prototype testing.

Output power	40 kW
Line-to-line rms voltage	380 V
Speed range	0 – 1000 r/min
Frequency range	0 – 50 Hz

It may be worth noticing that the relationship between the speed and the frequency does not depend on the overall number of poles of the machine as in the conventional design. Instead, it can be explained as follows: since the active region of the machine is practically the same as for a conventional double-side linear machine [9], we know that in a period T of the supply currents or voltages the track moves by two pole pairs. Looking at Figure 19, it appears that a track displacement by two pole pairs correspond to a wheel (and hence a shaft) rotation by 30 degrees, exactly as it happens in an ordinary six-pole rotating machine. Therefore, the 1000 r/min speed corresponds to a supply frequency of 50 Hz, as indicated in Table 2.

IV. PROTOTYPE MANUFACTURING

The motor prototype construction has been performed using custom-made processes and materials for all the components except rollers, bearings and track chains (Figure 15, Figure 16), which have been selected as high-reliability off-the-shelf components commercially available for industrial applications.

The stator cores are made of laser-cut silicon steel laminations with 0.50 mm thickness bonded and stacked together using the backlack technology [17]. This leads to intrinsically stable and robust laminated stacks (Figure 22) with no need for clamping plates and devices that would increase the machine dimension w indicated in Figure 14b. Figure 22 shows a single side laminated stator core endowed with slots for winding assembly and slots for interlock with the non-magnetic support (Figure 18) through dovetail joints. The finished stator cores are shown in Figure 23, where some details of the dual-layer FSCW implementation are also provided.

The manufacturing of the track elements (Figure 16) and of the side shields acting as track guides (Figure 15) required precision machining and mechanics to meet particularly tight tolerances. The material of track elements (ISO 10 B-2 steel) has been chosen to combine good mechanical performance and a high magnetic permeability, which is necessary to minimize the reluctance of the motor working flux paths (Figure 21). The permanent magnet integrated into each track element has been obtained from 5 elementary Neodymium-Iron-Bore segments for easier manufacturability and to minimize internal eddy current losses due to the large

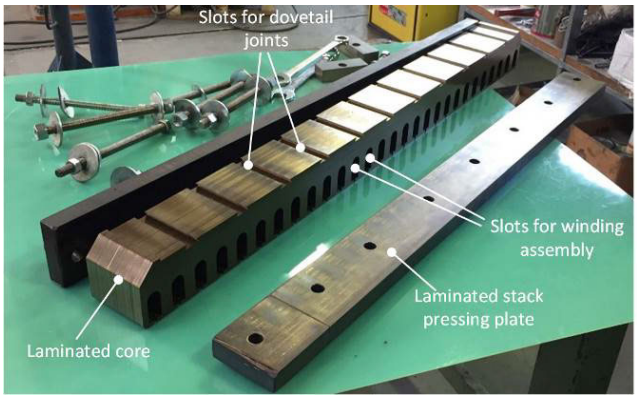

FIGURE 22. Single-side backlack laminated core with press-plates used for core manufacturing only.

FIGURE 23. (a) Wound stator core sections. (b) Stator winding overhang detail; (c) detail of electrical connections between coils.

space harmonics of the air-gap field produced by the stator FSCW [15].

A picture of the finished assembled prototype is shown in Figure 24. It can be observed that one of the two side shields is used to mount an encoder needed to measure the shaft position for speed control.

Overall, the manufacturing process of the prototype did not reveal any particular issue as regards the stator fabrication. The complete assembly process for the outer rotor proved to be challenging for the high number of components needed. On the other hand, the rotor modularity increased manufacturability in the sense that it allowed more elements to be fabricated in parallel before final assembly.

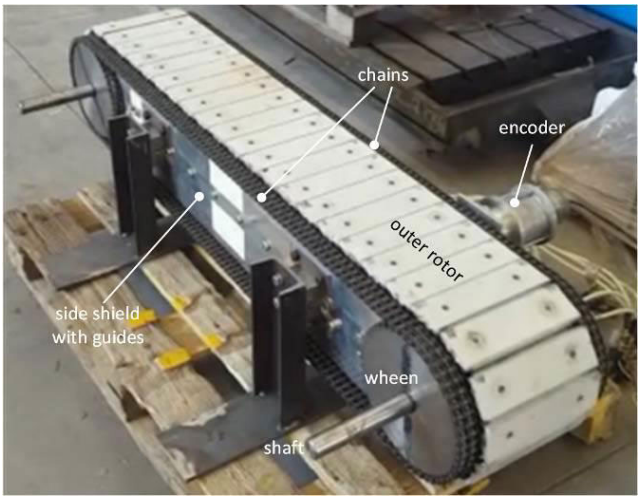

FIGURE 24. Assembled prototype equipped with the encoder for rotor position measurement and speed control.

V. PROTOTYPE TESTING

After a positive and complete factory test, the prototype has been mounted on a laboratory test bench for further validations. Pictures of the test bench and relevant equipment are provided in Figure 25.

A first check has been made on the machine operated as a driven generator at no load, comparing the measured back-ElectroMotive Force (EMF) with that obtained from FEA simulations (Figure 21a). The comparison is shown in Figure 26 and reveals a very good agreement, suggesting that, despite the unconventional machine structure, a 2D FEA simulation can suffice for a reasonably accurate performance prediction.

Of course, the no-load back-EMF appears remarkably distorted. Actually, this distortion does not result from the special machine topology, but is typical of some FSCW configurations also when implemented in conventional rotating machines [15]. In general, especially in inverter-fed motors not subjected to stringent torque ripple requirements, a similarly distorted back-EMF can be accepted with no significant detrimental effect on motor operation. Otherwise, it is well known from the literature that an electromagnetic optimized design combined with a suitable choice of the slot-pole combination for the FSCW can easily fix back-EMF distortion issues [15].

To assess the machine operation on load, the prototype has been loaded with an eddy-current brake coupled to one of the two shafts through a torque meter (Figure 25). For the electrical supply and speed control a Voltage Source Converter (VSC) (manufactuer: ABB, model ACS880-01-038A-4+C132+E200), has been used. The VSC is a standard off-the shelf model suitable for permanent-magnet synchronous motor supply implementing a Direct Torque Control encoder-less algorithm [18].

Throughout tests it has been possible to experimentally verify that, in spite of its strongly non-conventional design, the prototype could be effectively controlled through the employed standard VSC. For this purpose, it had been sufficient to use the same DTC control settings as for a normal 6-pole SPM motor.

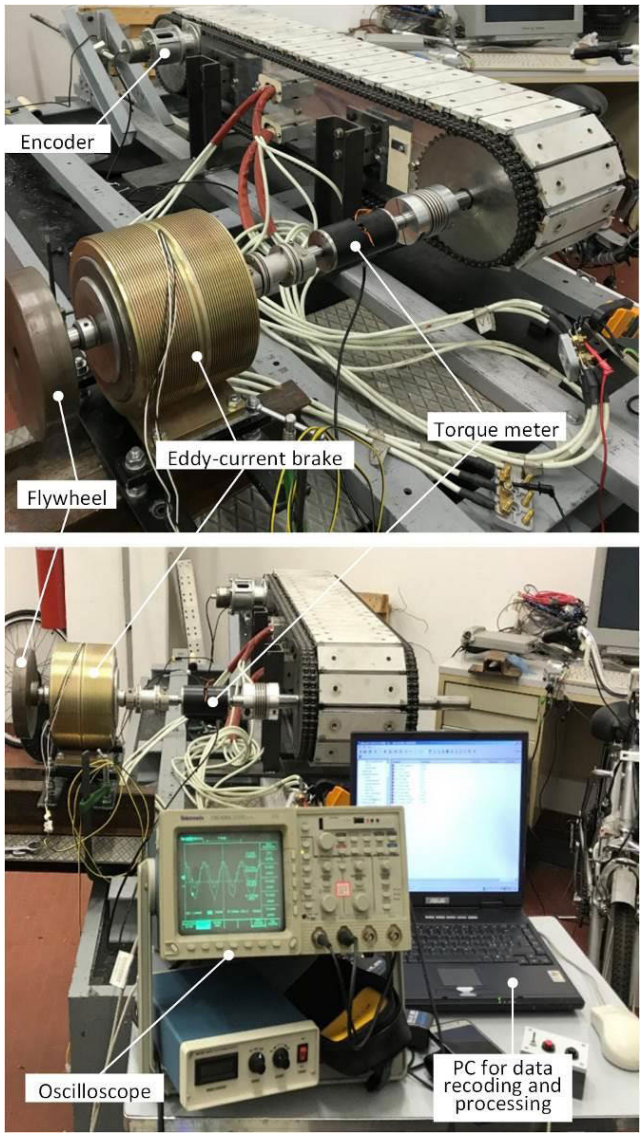

FIGURE 25. Test bench setup for prototype laboratory testing.

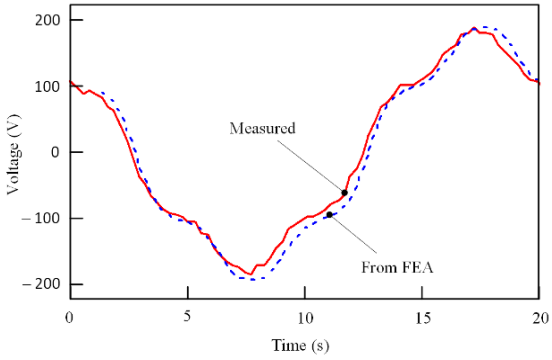

FIGURE 26. No-load Electro-Motive Force (EMF) at 1000 r/min from measurement and FEA simulation.

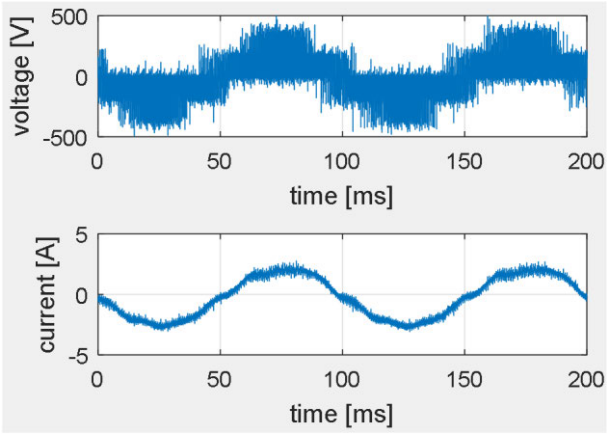

FIGURE 27. On-load voltage and current waveforms measured on the motor running at 200 r/min and delivering a torque of 50 Nm.

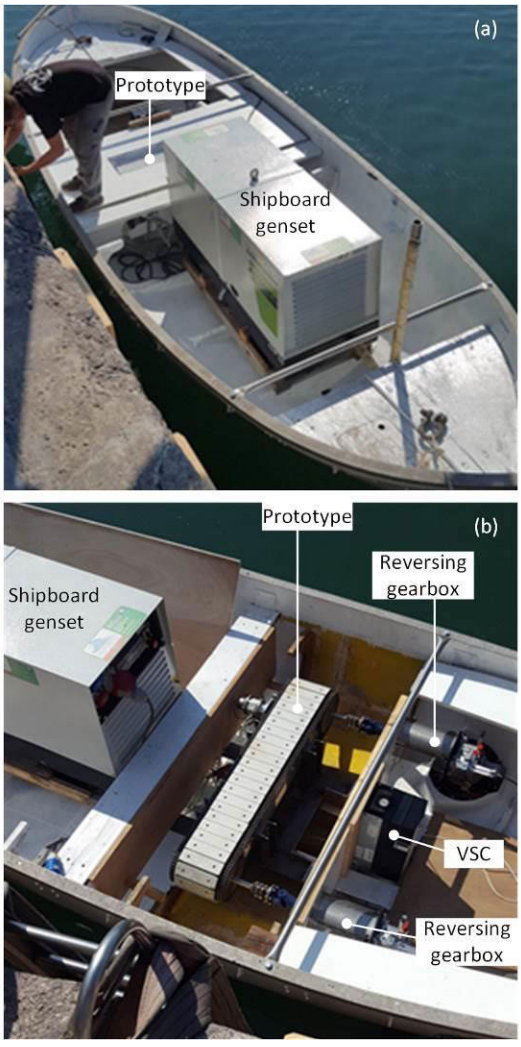

FIGURE 28. Setup for the prototype testing as a boat propulsion motor. (a) View with the motor embedded in a deck-embedded vane. (b) View after motor cover removal.

An example of voltage and current waveforms recorded on the machine operated as an inverter-fed motor is provided in Figure 27.

Thanks to the torque meter and wattmeter, it has been possible to obtain a direct measurement of the efficiency and losses at various speeds and torque. The measured data are provided in Table 3.

TABLE 3. Reference performance data assumed for prototype testing.

Speed (r/min)	Torque (nm)	Losses (W)	Efficiency (%)
100	386	2445	62.3
500	386	3760	84.2
750	386	4590	86.9
1000	386	5412	88.2

It can be seen that the majority of the losses are no-load losses and this causes the efficiency to remain relatively low even at higher loads compared to conventional machines. Furthermore, as it will be observed in the conclusion section, the most promising potentials for the machine topology under study can be envisioned in the field of direct-drive low-speed high-torque applications, wherein the efficiency is known to have a minor importance due to the low power levels involved [7]–[12].

In the framework of the research project aimed at developing the prototype, the equipment available for testing the machine in a shipboard operational environment has led to apply the VSC-fed motor as an electric traction drive for a dual-propeller boat. The test setup prepared for this purpose is illustrated in Figure 28.

In particular, the figure highlights how, thanks to its shape, the motor can be fit in a long thin vane below the deck, making it possible to exploit the whole space available between the two propeller shafts for torque production and to drive both shafts with the same machine. Such features may constitute a remarkable advance compared to conventional motor technology in case of severe space restrictions as pointed out in Section III.

The tests conducted on board showed a satisfactory overall performance including noise and vibrations aspects, showing that the proposed design is suitable for effectively reducing the mechanical issues found in the design and testing of the original proof-of-concept prototype (Section III.*A*.1). Furthermore, it has been confirmed that the machine is suitable for being effectively controlled by a standard VSC in all speed and load conditions allowed by the supply system capabilities and application needs. Of course, possible promising developments beyond the standard tested solution would encompass the implementation of fault diagnosis and fault tolerant control techniques according to the most current trends [19], [20].

VI. CONCLUSION

In this paper, the design, development, prototyping and testing of a new electric rotating motor topology with linear geometry specifically conceived for shipboard applications have been discussed as a follow-up of an original proof-of-concept technology demonstrator. The basic mechanical

issues which needed to be addressed in the machine development have been highlighted along with the design solutions adopted to solve them. Compared to a conventional rotating machine, the proposed technology introduces some structural complications due to the permanent-magnet outer rotor structure being composed of several independent rolling elements. However, significant advantages can be envisioned as well, thanks to the possibility that the new design offers to fit the motor in unusually shaped compartments as it is often needed on board in presence of severe space restrictions. The testing activities, performed both in factory and laboratory environments and using the machine as a boat propulsion motor, have shown an overall good performance, in particular proving the prototype suitability for being supplied and controlled by a standard off-the-shelf VSC. Possible shortcomings which have been pointed out by the prototype manufacturing and testing relate to a relatively complex mechanical construction possibly leading to increased volume, weight, noise, vibrations and reliability issues. However, all these drawbacks are significantly reduced in those application scenarios where the machine is employed as a low-speed torque motor, e.g. for the direct-drive actuation of heavy-duty shipboard loads like rudders, capstans, stabilizing fins, cable tensioners, etc. These utilization scenarios are envisioned as the most promising to fully exploit the proposed design potentials and minimizing its drawbacks. Future developments may concern the development of an effective cooling system to improve the machine continuous-service torque capability Moreover, feasibility studies are presently in progress for the possible application of the machine as a low-speed direct-drive wind generator to be installed inside wind towers. The linear structure of the machine, in fact, makes it very suitable for exploiting the large space available in the vertical direction within a wind tower for electromechanical energy conversion purposes. With respect to the usual arrangements (featuring a conventional generator fit into the nacelle), the solution would also exhibit promising advantages in terms of structural stability and weight distribution, in addition to allowing for a gearless arrangement thanks to the larger volume available in the wind tower compared to the nacelle. The analyses conducted so far confirm that the basic design choices made for the prototype described in the paper can be confirmed even when targeting higher torque values and larger machine dimensions, which suggest a good scalability of the proposed design.

ACKNOWLEDGMENT

The partners involved in the project were Lampas System, the University of Trieste, Cantiere Navale Quaiat and Area Science Park, Trieste, Italy. Special thanks are due to Mr. Angelo Torres and Mr. Alessandro Kalik from Lampas System for their invaluable contributions in terms of technical advice and leadership in prototype manufacturing and factory test. Mr. Marino Quaiat and Mrs. Gaia Benvenuti for their excellent work in making all needed equipment available for shipboard tests. Mr. Giorgio Contento from Concrane, Trieste, Italy, for his technical support in prototype testing. ABB for donating the electronic converter needed for prototype supply and variable-speed operation.

REFERENCES

[1] K. J. Binns and D. W. Shimmin, "Relationship between rated torque and size of permanent magnet machines," *IEE Proc. Electr. Power Appl.*, vol. 143, no. 6, pp. 417–422, Nov. 1996.

[2] J. Pyrhoonen, T. Jokinen, and V. Hrabovcova, *Design of Rotating Electrical Machines*. Hoboken, NJ, USA: Wiley, 2008, pp. 296–297.

[3] D. Mcmillan and G. W. Ault, "Techno-economic comparison of operational aspects for direct drive and gearbox-driven wind turbines," *IEEE Trans. Energy Convers.*, vol. 25, no. 1, pp. 191–198, Mar. 2010.

[4] J. Chen, D. Zhou, Z. Guo, J. Lin, C. Lyu, and C. Lu, "An active learning method based on uncertainty and complexity for gearbox fault diagnosis," *IEEE Access*, vol. 7, pp. 9022–9031, 2019.

[5] T. Li, T. Yang, Y. Cao, R. Xie, and X. Wang, "Disturbance-estimation based adaptive backstepping fault-tolerant synchronization control for a dual redundant hydraulic actuation system with internal leakage faults," *IEEE Access*, vol. 7, pp. 73106–73119, 2019.

[6] A. Bartnicki and A. Klimek, "The research of hydraulic pressure intensifier for use in electric drive system," *IEEE Access*, vol. 7, pp. 20172–20177, 2019.

[7] C. Bruzzese, A. Tessarolo, T. Mazzuca, and G. Scala, "A closer look to conventional hydraulic ship actuator systems and the convenience of shifting to (possibly) all-electric drives," in *Proc. IEEE Electric Ship Technol. Symp. (ESTS)*, Apr. 2013, pp. 220–227.

[8] M. Mezzarobba and A. Tessarolo, "Design and testing of a new linear topology for electric machines," in *Proc. 11th Int. Conf. Ecol. Vehicles Renew. Energies (EVER)*, Apr. 2016, pp. 1–6.

[9] A. Tessarolo and C. Bruzzese, "Computationally efficient thermal analysis of a low-speed high-thrust linear electric actuator with a three-dimensional thermal network approach," *IEEE Trans. Ind. Electron.*, vol. 62, no. 3, pp. 1410–1420, Mar. 2015.

[10] D. Zito, C. Bruzzese, M. Rafiei, E. Santini, T. Mazzuca, A. Tessarolo, and G. Lipardi, "Efficiency issues of a ship stabilizing fin assisted by a permanent magnet linear synchronous actuator," in *Proc. 12th Int. Conf. Electr. Mach. (ICEM)*, Lausanne, Switzerland, Sep. 2016, pp. 2633–2639.

[11] D. Zito, C. Bruzzese, A. Raimo, E. Santini, and A. Tessarolo, "A hybrid experimental drive concept of permanent magnet linear direct actuator servoed to a ship's hydraulic rudder," in *Proc. Int. Conf. Sustain. Mobility Appl., Renewables Technol. (SMART)*, Nov. 2015, pp. 1–8.

[12] D. Zito, C. Bruzzese, M. Rafiei, E. Santini, T. Mazzuca, A. Tessarolo, and G. Lipardi, "Actuation of ship stabilizing fins by a permanent magnet linear synchronous motor drive servoed to the hydraulic motor," in *Proc. 11th Int. Conf. Ecol. Vehicles Renew. Energies (EVER)*, Apr. 2016, pp. 1–7.

[13] S. O. Edhah, J. Y. Alsawalhi, and A. A. Al-Durra, "Multi-objective optimization design of fractional slot concentrated winding permanent magnet synchronous machines," *IEEE Access*, vol. 7, pp. 162874–162882, 2019.

[14] X. Fan, B. Zhang, R. Qu, D. Li, J. Li, and Y. Huo, "Comparative thermal analysis of IPMSMs with integral-slot distributed-winding (ISDW) and fractional-slot concentrated-winding (FSCW) for electric vehicle application," *IEEE Trans. Ind. Appl.*, vol. 55, no. 4, pp. 3577–3588, Jul. 2019.

[15] A. Tessarolo, C. Ciriani, M. Bortolozzi, M. Mezzarobba, and N. Barbini, "Investigation into multi-layer fractional-slot concentrated windings with unconventional slot-pole combinations," *IEEE Trans. Energy Convers.*, vol. 34, no. 4, pp. 1985–1996, Dec. 2019.

[16] A. Tessarolo, F. Luise, S. Pieri, A. Benedetti, M. Bortolozzi, and M. De Martin, "Design for manufacturability of an off-shore direct-drive wind generator: An insight into additional loss prediction and mitigation," *IEEE Trans. Ind. Appl.*, vol. 53, no. 5, pp. 4831–4842, Sep. 2017.

[17] K. Bourchas, A. Stening, J. Soulard, A. Broddefalk, M. Lindenmo, M. Dahlen, and F. Gyllensten, "Quantifying effects of cutting and welding on magnetic properties of electrical steels," *IEEE Trans. Ind. Appl.*, vol. 53, no. 5, pp. 4269–4278, Sep. 2017.

[18] F. Niu, B. Wang, A. S. Babel, K. Li, and E. G. Strangas, "Comparative evaluation of direct torque control strategies for permanent magnet synchronous machines," *IEEE Trans. Power Electron.*, vol. 31, no. 2, pp. 1408–1424, Feb. 2016.

[19] Y. Wu, B. Jiang, and N. Lu, "A descriptor system approach for estimation of incipient faults with application to high-speed railway traction devices," *IEEE Trans. Syst., Man, Cybern. Syst.*, vol. 49, no. 10, pp. 2108–2118, Oct. 2019.

[20] Y. Wu, B. Jiang, and Y. Wang, "Incipient winding fault detection and diagnosis for squirrel-cage induction motors equipped on CRH trains," *ISA Trans.*, vol. 99, pp. 488–495, Sep. 2019, doi: 10.1016/j.isatra.2019.09.020.

MARIO MEZZAROBBA received the Laurea degree in electrical engineering from the University of Trieste, Trieste, Italy, in 2009, and the Ph.D. degree in electrical engineering from the University of Padova, Padova, Italy, in 2014. Since 2014, he has been a Research Fellow with the University of Trieste. He has actively taken part in several research projects for the dimensioning, design, prototyping, and testing of electromechanical actuators, components, and systems. His main research interests include induction motor, permanent-magnet machine and electromagnetic stirring analysis, and design and optimization.

ALBERTO TESSAROLO (Senior Member, IEEE) received the Laurea degree in electrical engineering from the University of Trieste, Italy, in 2000, and the Ph.D. degree in electrical engineering, Padova, Italy, in 2011. He worked in design and development of large innovative motors, generators, and drives. Since 2006, he has been with the Engineering and Architecture Department, University of Trieste, where he teaches the courses of electric machine fundamentals and electric machine design. He leads several funded research projects in cooperation with industrial companies for the study and development of innovative electric motors, generators and drives. He has authored over 150 international articles in the area of electrical machines and drives. He is a member of the Rotating Machinery Technical Committee (TC2) of the International Electrotechnical Commission (IEC), the IEEE Power and Energy Society Electric Machinery Committee, the IEEE Industry Applications Society Electric Machines Committee, and the IEEE Industrial Electronics Society Electric Machines Technical Committee. He served as an Associate Editor for the IEEE TRANSACTIONS ON ENERGY CONVERSION, the IEEE TRANSACTIONS ON INDUSTRY APPLICATIONS, and *IET Electric Power Applications*. He serves as the Editor-in-Chief for the IEEE TRANSACTIONS ON ENERGY CONVERSION.

NICOLA BARBINI received the Laurea degree from the University of Trieste, Italy, in 2012, where he is currently pursuing the Ph.D. degree in electrical engineering. His research interests include modeling and analysis of electric machines, and power transformers.

SIMONE CASTELLAN received the Laurea and Ph.D. degrees in electrical engineering from the University of Padova, Padova, Italy. In 2000, he joined the University of Trieste, Trieste, Italy, as a Researcher, dealing with electric power converters, machines, and drives, where he is currently an Assistant Professor of power electronics. His research interests include power converters for harmonic, flicker and reactive power compensation, medium-voltage drives, fault-tolerant drives, all-electric ships, and vehicle-to-grid systems.

BARBARA CODAN received the Laurea degree in materials engineering and the Ph.D. degree in nanotechnology from the University of Trieste, Trieste, Italy, in 2005 and 2009, respectively, and the Executive Master in Business Administration degree with the MIB Business School, Trieste, in 2015. She spent five years as a Research Fellow. In 2016, she joined Lampas System, as an Innovation Manager, taking part in various research projects.

MARTINA TERCONI received the Laurea degree in chemical engineering from the University of Trieste, Trieste, Italy, in 2003. Since 2005, she has been with the Area Science Park, as a Technology Expert of regional, national, and international technology transfer projects. She was a Technology Broker, especially for those concerning research and development, and technology transfer of new materials and innovative technologies.

CLAUDIO BRUZZESE (Senior Member, IEEE) received the M.Sc. *(cum laude)* and Ph.D. degrees from the Sapienza University of Rome, Rome, Italy, in 2002 and 2008, respectively. He was with National Power System Management Company. From 2002 to 2011, he was with the Department of Astronautic, Electrical, and Energy Engineering, Sapienza University of Rome, as an Assistant Researcher. Since 2011, he has been an Assistant Professor with the Sapienza University of Rome, where he teaches the courses of electric machines and electric machine design. He is also a consultant with the Italian Ministry of Defense for various research projects.

AUGUSTO FUSARI received the Diploma degree in electrical engineering, Bergamo, Italy, in 1985. In 1986, he joined Tecnomasio Brown Boveri, as a Site Manager. Throughout his career, he supervised test rooms for trucks and cars with Iveco and Fiat, and construction sites abroad of bar and wire rod mills for cold mill and hot mill plants. Since 1995, he has been an Application Manager with ABB, Sesto San Giovanni, Italy, in the electric drive sector, where he mainly deals with power electronics and drive converters for nonconventional applications.